Altitude Correction of an UAV Assisted by Point Cloud Registration of LiDAR Scans

Marcus Davi Forte[1], Polycarpo Souza Neto[2], George André Pereira Thé[2] and Fabricio Gonzalez Nogueira[1]

[1]*Department of Electrical Engineering, Federal University of Ceara, Fortaleza CEP 60455-970, Brazil*

[2]*Department of Teleinformatic Engineering, Federal University of Ceara, Fortaleza CEP 60455-970, Brazil*

Keywords: Unmanned Aerial Vehicle, Localization, Laser Scanning, Generalized Iterative Closest Point, Fast Point Cloud Registration, Stockpile Mapping.

Abstract: This paper presents an online localization estimation of an Unmanned Aerial Vehicle (UAV) by fusing data provided by the on-board flight controller and a LiDAR (Light Detection and Ranging) carried by the UAV. Pose estimations solely obtained by the UAV are often corrupted by noise or instrumentation limitation, which may lead to erroneous mapping of the environment. To correct potential estimation errors, the LiDAR scans are assembled into a local point cloud history and matched against a partial map of the environment using a proposed point cloud registration method, similar to a Simultaneous Localization and Mapping (SLAM) approach. The resulting correction is incorporated into the estimation of the UAV using an asynchronous Kalman Filter implementation. For this work, only the altitude errors are corrected by the registration. We conducted tests on a local thermal power plant which contained three large coal stockpiles. We chose one of them as our Region of Interest (ROI).

1 INTRODUCTION

The mapping procedure and modeling of three dimensional objects is a subject of interest of various applications, for example precision agriculture (Lin and Habib, 2021). The precise reconstruction of real surfaces has become a challenge and has been deeply studied over last years (Vacca et al., 2018), and the use of UAV (Unmanned Aerial Vehicle) as a remote sensing platform has shown promising results.

It is essential that the UAV carrying sensory instrumentation such as cameras or Light Detection and Ranging (LiDAR) sensors provides accurate estimates for its three dimensional pose. The sensory data provided by the on-board instrumentation is usually associated to the pose of the aircraft. Any uncertainty present in the pose estimation directly affects the quality of the information inferred from the sensor (Mughal et al., 2021). UAV often relies on Global Navigation Satellite System (GNSS) combined with Inertial Measuring Units (IMU). However, GNSS signals are vulnerable to noise and IMU is not reliable for long-term estimations. Consequently, whenever a GNSS signal suffers from some interference, it affect the entire pose estimation of the UAV. A less noisy estimation alternative is the use of Real Time Kinematic (RTK) equipment, which is able to offer estimations with less than 5 *cm* error. Such solutions, however, are much more expensive than GNSS solutions.

These drawback motivates the use of the on-board instrumentation of the UAV to help correct estimation errors that arise from the localization sensors. In (Mughal et al., 2021) a deep learning technique is used on image from cameras to localize an UAV based on geotagged images. The approach is, however, unable to provide real time estimates and require training data before usage. On the other hand, LiDAR sensors are able to provide common landmarks between scans so that the motion of the aircraft is successfully estimated in real time, as explored in (Chiang et al., 2017). This technique is usually integrated into a Simultaneous Localization and Mapping (SLAM) framework. The scan matching between frames is achieved by applying what is known as point cloud registration.

In this work, we will explore the use of point cloud registration for estimating the error on the altitude of an UAV in real time. We will present experimental results and an implementation of an asynchronous Kalman filter for integrating the estimations.

Forte, M., Neto, P., Thé, G. and Nogueira, F.
Altitude Correction of an UAV Assisted by Point Cloud Registration of LiDAR Scans.
DOI: 10.5220/0010583004850492
In *Proceedings of the 18th International Conference on Informatics in Control, Automation and Robotics (ICINCO 2021)*, pages 485-492
ISBN: 978-989-758-522-7

2 LITERATURE REVIEW

2.1 UAV-based Laser Scanning

LiDAR based UAV scanning system is an alternative solution to the classical photogrammetry method of acquiring a 3D model of surfaces. The laser methods can be applied to mitigate gaps and acquire a precise point cloud image (Huang et al., 2019). It can offer a centimeter accuracy and the data capture can be performed either aerial or terrestrial (Amann et al., 2001). It has been shown that such approach produces slightly superior accuracy results comparing to photogrammetry methods (He et al., 2019).

Recent works have been utilizing LiDAR sensors to acquire 3D point clouds of bulk material stockpiles. The works (Zhang et al., 2020; He et al., 2019) present solutions for the laser scan measurement of stockpiles using mobile hand-held devices that needs to be carried along with the entire stockpile surrounding. This technique has the limitation that it can only capture a side view from the stockpile, essentially missing information about the top side of higher piles. In addition, the data acquisition is a slow process and can cause physical stress for the person carrying the scanner system the whole stockpile, not to mention that the carrier is exposed to perilous conditions during the acquisition procedure due to the existing coal particulates and pile collapse risk.

Equipping a similar system to a UAV overcomes several of these difficulties. The aerial systems have the advantage of covering large areas or places that are not easily accessible for terrestrial systems. Some works have successfully integrated LiDAR sensors into UAVs in order to construct 3D point cloud data. In (Wallace et al., 2012) a low-cost UAV-LiDAR system was developed for managing forest inventories. Data fusion algorithms that combine Global Positioning System (GPS), IMU and video camera images are employed to UAV position and posture estimation during the flight.

In (Beland et al., 2019) is presented the use of a LiDAR sensor in an airborne covering large areas and acquiring a large amount of data. Airborne LiDAR remote sensing systems must be able to provide accurate aircraft position information. Otherwise, the formed point cloud will present unreliable information. Measurement errors and attitude fluctuations affect the accuracy of laser points, and the impacts of these problems are discussed in (Wang et al., 2011), (Wang et al., 2018), and (Hauser et al., 2016).

2.2 Point Cloud Registration

The Iterative Closest Point (ICP) algorithm was proposed in (Besl and McKay, 1992) and aims at finding a transformation that optimizes a rotation and translation in two point clouds. The algorithm uses one of the data sets a reference and applies rotations and translations to the other set. This is repeated iteratively until the convergence occurs, that is, the smallest difference between the gradient of two successive iterations. Although it is widely used in the literature, as it has an iterative method and depends on an initial guess, it is quite susceptible to local minimums. In (Chen and Medioni, 1992), an improvement is made in the ICP, where we now have information on the surface normal, called the point to plane ICP. However, this approach fails to deal with clouds of different densities, with many outliers or noise, which somehow affects the calculation of the normal.

An efficient approach to registration dense clouds is the GICP (Segal et al., 2009). This probabilistic version of the ICP is based on the probabilistic Maximum Likelihood Estimation model (MLE). The method explores local planar patches in both point clouds. For this case, we say that the metric here is a generalization of the point to point and point to plane metrics, with the concept of plane to plane being introduced. As a failure, the GICP has a reasonably high computational cost compared to other ICP variants.

In the search for an alternative to conventional sampling methods and the attempt to reduce ambiguities, computational cost and obtain better alignment, the Cloud Partitioning ICP (CP-ICP) method was proposed in (Souza Neto et al., 2018). Basically, the two clouds involved in the process are partitioned into the same number of slices, with each pair (slices of the same index) subject to registration and the best alignment among the various pairs, represents the rigid transformation that best corrects the entire clouds (since which are rigid bodies).

In view of the problems found in the classic algorithms, sometimes the quality of the alignment, in other situations due to the high computational cost, this work proposes the utilization of a modified version of CP-ICP algorithm with the purpose of correcting erroneous height estimates provided by an UAV pose estimation in real time. We will see more details in the following section.

3 PROPOSED MATCHING

3.1 Cloud Partitioning Generalized ICP (CP-GICP)

Recently, it was proposed a subsampling stage of point clouds, where two sets of data, both were partitioned into k parts, in order to reduce the computational cost for the alignment step.(Souza Neto et al., 2018). This partitioning step is previous to the alignment, performed on the partitions by the ICP algorithm (Besl and McKay, 1992). In summary, the partitions of the source cloud (S) are aligned with those of the target cloud (M), where the rigid transformation that results from this alignment is replicated in the complete source cloud, correcting its pose in relation to the reference. The equation that represents the alignment of the partitions, using the CP-ICP method in (Souza Neto et al., 2018) can be seen in Eq. 1.

$$E_j(\Psi)_{ICP} = \frac{k}{N}\sum_{i=1}^{\frac{N}{k}} \parallel \vec{m}_i - \Psi\vec{s}_i \parallel, \qquad (1)$$

where j they are the indexes of the partitions being aligned, N it is the number of points, $\vec{s}_i$ it is i-th vector related to the source point cloud, $\vec{m}_i$ the i-th vector related to the target point cloud and Ψ it is the rigid transformation (4 x 4 matrix) obtained from ICP in the alignment core.

In this paper, we propose some changes to the previously mentioned algorithm, in order to adapt it to the purpose of this work. In the current version of the algorithm, the first modification we added a density equalization step, as a first level of sampling. After that, will be separate only one of the point clouds into smaller parts hereinafter referred to as sub-clouds, and then perform the registration process for each partition with the other entire cloud, until a simple decision criterion (here the lowest possible RMSE compared to a criterion decided a previously) is reached. It is worth mentioning that this variant of the algorithm with a second modification, intrinsic to the needs of the application, where here, the alignment core is Generalized ICP (Segal et al., 2009), suitable for the alignment of outdoor scenarios. The equation that describes the proposed alignment method is seen in Eq. 2.

$$E_j(\Psi)_{GICP} = \frac{k}{N}\sum_{i=1}^{\frac{N}{k}} d_i^{(\Psi)^T}(\Sigma_i^{M_j} + \Psi\Sigma_i^{S_j}\Psi^T)^{-1} d_k^{(\Psi)}, \qquad (2)$$

where $d_i^{(\Psi)^T}$ they are point to point distances of the correspondences, $\Sigma_i^{S_j}$ and Σ_i^{M} are covariances of the local point neighborhoods of j-th source sub-cloud and target point cloud, respectively.

The choice to partition only one of the clouds is due to the size discrepancy between the data involved in the process; in relation to the alignment core, GICP error metric that generalizes over point to point and point to plane, it uses covariances of the local point neighborhoods in order to align the underlying surfaces rather than the points themselves (Holz et al., 2015). The classic ICP, used in the variant improved CP-ICP is known for its susceptibility to the problem of local minimums. Because it is an iterative method, it requires an initial guess, without which the algorithm can easily get stuck in a local minimum (Yang et al., 2016). If this occurs, the solution may be far from the optimal solution, resulting in an incorrect estimate. This interpretation of the above can be seen in Figure 1(a) and 1(b).

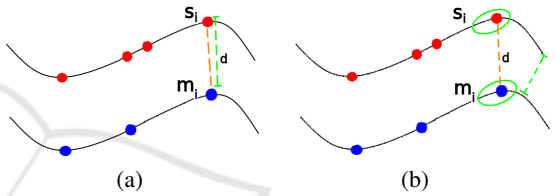

Figure 1: Error metrics and transformation estimators. In (a) point to point erro metric and (b) Generalized ICP or plane to plane error.

3.2 Sufficient Registration

Consider two point clouds: an source point cloud and a target point cloud. The goal is to successfully perform a registration procedure, which means matching the input point cloud to the target one. Let is see the steps:

1. Initially, we performed density equalization of the point clouds, using a voxel grid algorithm;
2. Subdivide one of the datasets (the source) in k sub-clouds;
3. For each of the k iterations, solve the Generalized ICP algorithm for the partition and the entire target cloud:

- Apply the achieved transformation to the source point cloud;
- The source cloud post GICP is then compared to the target point cloud, using RMSE error at each iteration;
- If the RMSE value achieved in a given iteration is acceptable (when it compares to a stop criterion) the algorithm stops and the ideal transformation has been found.

4 LASER-BASED UAV SCANNER SYSTEM

The aerial scanning system is mainly composed of an industrial UAV and an embedded computer which implements the proposed pose compensation system.

The DJI Matrice 100 is a fully programmable quad-copter. It features an Onboard Software Development Kit (OSDK) which allows sensor data sampling in real-time, setting missions and waypoints, and creating flight reports. Its weight is around 2.5 kg and can carry an additional 1.1 kg as payload. It comes with IMU and GPS to estimate its position and orientation. The provided SDK allows direct integration with the ROS framework. Any ROS-Supported embedded computer is able to communicate with the Matrice 100 though a serial port made available within the drone frame.

Once SDK is installed in the embedded computer, it provides an application that offers topics containing useful information, among them, the most important are the fused geographic coordinate and the fused orientation data. The coordinates are the result of a proprietary data fusion algorithm that combines data from IMU and GPS. The resulting data is also a geographic coordinate, containing more accurate latitude, longitude, and altitude information. Coming from the IMU, and magnetic compass, a fused orientation is also provided. Both 3D coordinate and 3D orientation data are published in topics with a programmable frequency of up to 50 Hz.

The chosen embedded computer is an Asus Tinker Board S with a Debian-based distribution which supports ROS framework. It is powered by a quad-core ARM based processor, with 16 GB eMMC storage, 2 GB of LPDDR3 dual-channel memory, and operates at frequencies up to 1.8 GHz. Its main role is to act as an interface between the drone and the LiDAR sensor to assemble the point cloud data.

The used LiDAR is a SICK LD-MRS420201 designed for outdoor applications. It has IP69K enclosure rate protection and weights 0.77 kg. Its scanning range stands under 150 m and 50 m for objects up to 90% and 10% remission, respectively. And coal is a material with low levels of remission. Therefore the LiDAR is expected to work with a range of up to 50 m. The sensor possesses ROS drivers for integration with ROS applications, which are essential for point cloud models assembly. The sensor is attached beneath the drone and points towards the ground during the flight.

5 REGISTRATION-ASSISTED LOCALIZATION ESTIMATION

This section details the proposed system for correcting measurements using point cloud registration.

The UAV is able to provide a full pose estimation using inertial sensors, GNSS localization and the model of the drone itself. As stated in the documentation of the equipment, this estimation contains an estimation error of about a few meters. We propose a Kalman filter structure which models the noise error and receives the correction of the point cloud registration as an update variable.

Figure 2 illustrates the estimation process. First, the map is constructed using the pose from the UAV instrumentation. The map construction performed using frame transformations from an inertial frame, whose origin is set to the take off position. and the laser frame. As the UAV flies above the surface, the laser point clouds are transformed to the map frame and added to the previous ones. Notice that during this step, it is not possible to correct the UAV pose.

As soon as the UAV detects an overlap between the current laser scan and the map, it is assumed that the overlap is enough to provide a correction estimation. The registration process is then triggered and the output transformation matrix is used to provide the height correction. Subsequent laser scans are added to the current map but with the corrected pose.

We included a parameter χ, defined as the local point cloud history, which controls how many laser scans are included in the source point cloud used for the registration.

5.1 Asynchronous Kalman Filter

A Kalman filter structure is modeled to account for the asynchronous registration corrections and the estimation provided by the DJI proprietary fusion solution. The term asynchronous refer to that fact that the corrections occur at a variable sampling rate, in contrast to the predictions which occur at a constant sampling rate. The equations remain the same, but the implementation is slightly different. Instead of executing both predictions and corrections in a single iteration, the correction step is called only upon receiving the updating states provided by the point cloud registration. Moreover, it is possible to use multiple corrections models, each with its own measurement matrix and sampling rate (Shabani et al., 2015).

Since we do not have access to the UAV estimation internal model, the proposed Kalman Filter treats the incoming data from the UAV estimation as an update measurement. The corresponding measurement

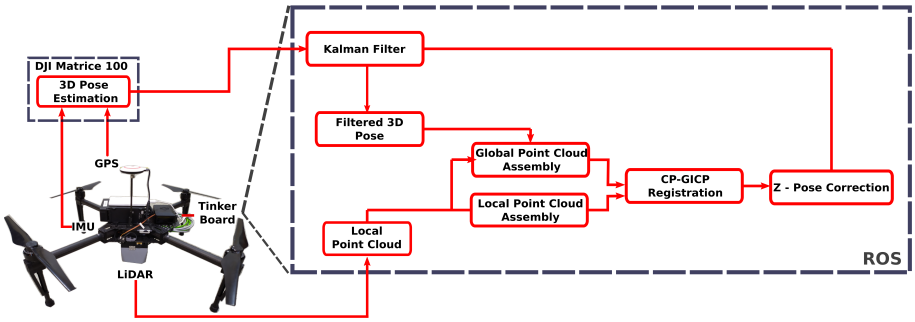

Figure 2: Flowchart of registration-assisted localization.

noise covariance is then computed through the accuracy given by the equipment data sheet.

The correction transformation estimation is also treated as an update measurement. Note that the transformation matrix is an 4×4 matrix, composed of a rotation component and a translation component. This work will focus only on the translational z component. This correction is extracted from the resulting registration matrix and fed into the Kalman filter update equation.

Therefore, the states which will be estimated by the filter are given by

$$x = \begin{bmatrix} x & y & z & \delta z \end{bmatrix}^T, \tag{3}$$

where x, y and z is the three dimensional pose of the UAV and δz is the measurement error on z.

The Kalman Filter algorithm is implemented in two steps, the prediction and the update. We assume that the process and measurements noises are modeled by a Gaussian distribution with zero mean. The computation of the state prediction is given by

$$\hat{x}_k^- = A\hat{x}_{k-1} + Bu, \tag{4}$$

$$P_k^- = AP_{k-1}A^T + Q_n, \tag{5}$$

where x is the estimated state, A is the state transition model, B is the input model, u is the input vector, P is the covariance of the estimation error and Q_n is the covariance of the process noise. The computation of the state updates, or state innovation, is given by

$$\tilde{e}_k = y_k - C\hat{x}_k^- \tag{6}$$

$$S_k = CP_k^-C^T + R_n \tag{7}$$

$$K_k = P_k^-C^TS^{-1} \tag{8}$$

$$\hat{x} = \hat{x}_k^- + K_k\tilde{e}_k \tag{9}$$

$$P_k = (I - K_kC)P_k^-, \tag{10}$$

where $\tilde{e}_k$ is the prediction error, y_k is the measured output, C is the output model matrix, R_n is the measurement covariance matrix and K_k is the Kalman gain matrix.

5.2 Implementation

Our implementation of the Kalman filter contains two separate update steps, one from the estimated pose incoming from the sensory instrumentation of the UAV and another from the registration correction. Thus, we compose two different C matrices

$$C_1 = \begin{bmatrix} 1 & 0 & 0 & 0 \\ 0 & 1 & 0 & 0 \\ 0 & 0 & 1 & -1 \end{bmatrix}, \tag{11}$$

which models the estimation and includes the altitude model error δz compensated in the measured z, and

$$C_2 = \begin{bmatrix} 0 & 0 & 0 & 1 \end{bmatrix}, \tag{12}$$

which yields the estimated altitude error δz.

For this particular case, the prediction step (4) is not performed. We compute only the update in the estimated covariance error (5) according to the noise covariance Q_n which models the instrumentation noise. This computation is calculated every time the pose is updated.

At the same time, update equations (6)-(10) corresponding to C_1 is computed. This step uses its own measurement noise covariance R_{n1}.

As soon as the registration subsystem outputs its correction estimate, the same update equations (6)-(10) are computed, this time using the corresponding noise R_{n2}.

The measurement covariance matrix R_{n1} is related to the UAV instrumentation, while matrix R_{n2} is related to the performance of the registration and how much time has passed without any correction, since we assume the uncertainty increases with the time. For this work, we assume it to be a constant matrix scaled by the time between registration corrections.

6 EXPERIMENTAL RESULTS

The developed system was evaluated through field tests carried out in a real stockyard (Figure 3) with a coal stock capacity of approximately 600 thousand tons. The plant is located in the state of Ceará – Brazil and is part of the Pecem Thermoelectric Complex (Pecem TC), with an installed capacity of 1080 MW of active power. There are a total of three stockpiles within the power plant. We chose one of the for our experiments.

Figure 3: UAV in a thermal power plant.

The UAV was programmed to fly over the chosen stockpile by setting four waypoints to be tacked by the flight controller, as shown in Figure 4.

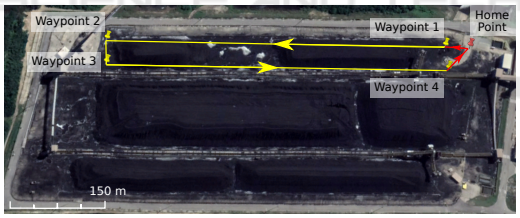

Figure 4: Home point and waypoints used on the experiments.

During the tracking of Waypoint 1 towards Waypoint 2, the UAV was set to build the map using only the estimates from the instrumentation, without any registration correction, since there is still no overlapping region between scans and a map. During the tracking of Waypoint 3 towards Waypoint 4, we enable the registration procedure. During this period, the local point cloud history is matched against the previously acquired map in order to estimate deviation in the altitude. The correction is then applied to the current altitude and the frame of the UAV is updated. The resulting corrections are shown in Figure 5.

Notice how the altitude error varies over time and may reach up to 3.5 m. The error be better visualized in Figure 6.

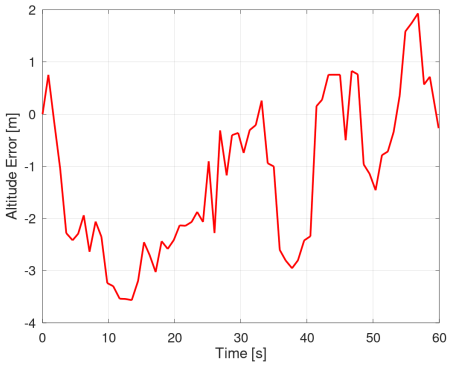

Figure 5: Result of registration-assisted altitude correction.

6.1 Comparison between Registration Algorithms

We implemented a variant registration approach to CP-ICP, in C ++, with the aid of the PCL library, without code optimization, and we conduct experiments of alignment, simulating accumulation of data in three different sizes of histories, thus comparing the proposed method to CP-ICP and other classic algorithms, focused on the alignment of outdoor scenes.

The comparison with the state of the art is carried out between the point to point and point to plane ICP variants, the Generalized ICP, CP-ICP and the proposed method. The metrics used for comparison are the smallest possible rotation and displacement to be achieved, $\varepsilon_R = arccos(\Delta R - I)/2$ (in degree) and $\varepsilon_T = \mu_c - \mu_s$ (where μ_c and μ_s are respectively the centroides of the registered source cloud and the original source cloud) and the time (in seconds), which for applications in real time must be as small as possible.

Table 1 synthesizes the rotation, translation and cost time performance of the various registration approaches; as it is clear from the results, the proposed method achieved top performance for each 3D model aligned. A good performance of the proposed approach confirms to some extent the expectations about computational cost reduction due to partitioning and density reduction through sampling with voxel grid, a correct alignment by changing the alignment core, performing small rotations, since the rotation error here should be close to zero, in addition to a perfect altitude correction. When compared to the others, we conclude that the classic ICP make mistakes due to bad estimates, as well the CP-ICP itself. Among those used for comparison, only the GICP can achieve very close results, however two orders of magnitude are more costly.

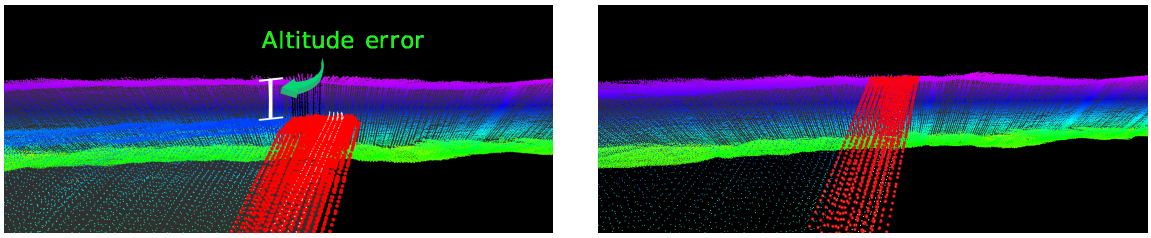

(a) (b)

Figure 6: Side view of a history registration. In (a) the initial pose, with difference in altitude and in (b) alignment with the proposed method.

Table 1: Table with comparison metrics for the Stockpiles scenes registration.

	Scan 1			Scan 2			Scan 3		
	$\varepsilon_R(o)$	$\varepsilon_T(m)$	t (s)	$\varepsilon_R(o)$	$\varepsilon_T(m)$	t (s)	$\varepsilon_R(o)$	$\varepsilon_T(m)$	t (s)
ICP_{p2pt}	59.1370	3.8866	6.8892	43.9945	1.2401	13.0223	42.2599	0.9203	19.2812
ICP_{p2pl}	50.488	4.3514	3.3678	40.0173	2.5921	5.1246	35.9679	2.4285	6.7039
GICP	0.7244	2.1613	60.1746	0.7593	1.7940	61.5916	1.2170	1.5967	70.1895
CP-ICP	27.4122	0.7217	1.4764	26.6329	-0.1478	2.8011	28.3209	-0.9307	4.1855
Proposed	**0.6370**	**1.9936**	**0.5744**	**0.8080**	**1.7688**	**0.6042**	**0.2676**	**1.5011**	**0.6377**

More deeply evaluating the algorithms, some factors, as the parameters set can influence. Particularly we can mention as a factor of the choice of the GICP instead of the ICP (for alignment core) the low tuning sensitivity of the maximum distance for correspondence. Generally, if this value is very small, the probability of convergence to an undesired local minimum is high and the number of iterations to correct the pose can increase. If this distance is too high, the transformation estimation may suffer with a loss of accuracy. In the present work, our main problem is the altitude correction, which contemplates this failure of the ICP.

In Figure 6, we have an example of a side view of a clearly misaligned history, in 6(a), and the result of the pose correction by the proposed algorithm, in 6(b).

6.2 Volume Estimation

Stockpile inventory control is an extremely important process of the thermal power plant. The plant must know how much coal they posses before issue any purchase, selling or usage in the plant itself. The point cloud generated by our experiments may be used to give such important estimate. This estimate will also be used to evaluate the performance of the mapping and the impact caused by misaligned point clouds. Figure 7 shows the top view of a cropped point cloud corresponding to satellite image from Figure 4. A ROI (Region of Interest) cropping was applied over part of the stockpile.

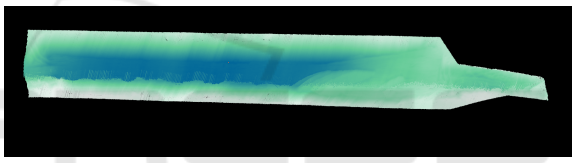

Figure 7: Top View of ROI.

The volume was computed using an algorithm that applies a gridding process and sums the volume differences between the highest point in the cloud and an arbitrary ground surface. We then set the same ground plane for the resulting point clouds of the mapping with and without registration and computed the corresponding volumes, as shown in Table 2.

Table 2: Estimated volumes.

Point Cloud	Volume (m^3)
Without Altitude Correction	60243.67
With Altitude Correction	**54467.18**

Notice that the misaligned point cloud yields a volume error over 10%. This is a significant amount, considering that erroneous stockpile estimates may heavily affect the purchase and usage of the material within the power plant.

7 CONCLUSION

Among the contributions of this work, we present an approach for the registration of point cloud of external scenarios. The proposed algorithm takes the Generalized ICP to a new use, aligning doubly subsampled data. In comparison with other algorithms, the low computational cost derives from the reduction of density by the voxelgrid and the space of the sub-clouds of one of the sets. In terms of accuracy, changing the alignment core, using the Generalized ICP instead of the classic ICP (as in CP-ICP), we avoid convergence to local minimums. We then use the proposed registration approach for correcting the altitude of the UAV in real time. The corrections allowed the subsequent mapping to be aligned to the existing map, which helps constructing a more reliable dataset that represents the actual stockpile surface.

ACKNOWLEDGEMENTS

This study was financed in part by the Coordenação de Aperfeiçoamento de Pessoal de Nível Superior-Brazil(CAPES)-Finance Code 001; Financial support from Energia Pecem and ANEEL under the grant number PD-07267-0016/2018.

REFERENCES

Amann, M.-C., Bosch, T. M., Lescure, M., Myllylae, R. A., and Rioux, M. (2001). Laser ranging: a critical review of unusual techniques for distance measurement. *Optical Engineering*, 40(1):10 – 19 – 10.

Beland, M., Parker, G., Sparrow, B., Harding, D., Chasmer, L., Phinn, S., Antonarakis, A., and Strahler, A. (2019). On promoting the use of LiDAR systems in forest ecosystem research. *Forest Ecology and Management*, 450:117484.

Besl, P. J. and McKay, N. D. (1992). Method for registration of 3-d shapes. *IEEE Transactions on Pattern Analysis and Machine Intelligence*.

Chen, Y. and Medioni, G. (1992). Object modelling by registration of multiple range images. *Image and vision computing*, 10(3):145–155.

Chiang, K., Tsai, G., Li, Y., and El-Sheimy, N. (2017). Development of LiDAR-based UAV system for environment reconstruction. *IEEE Geoscience and Remote Sensing Letters*, 14(10):1790–1794.

Hauser, D., Glennie, C., and Brooks, B. (2016). Calibration and accuracy analysis of a low-cost mapping-grade mobile laser scanning system. *Journal of Surveying Engineering*, 142(4):04016011.

He, H., Chen, T., Zeng, H., and Huang, S. (2019). Ground control point-free unmanned aerial vehicle-based photogrammetry for volume estimation of stockpiles carried on barges. *Sensors*, 19(16):3534.

Holz, D., Ichim, A. E., Tombari, F., Rusu, R. B., and Behnke, S. (2015). Registration with the point cloud library: A modular framework for aligning in 3-d. *IEEE Robotics & Automation Magazine*, 22(4):110–124.

Huang, R., Jiang, L., Wang, H., and Yang, B. (2019). A bidirectional analysis method for extracting glacier crevasses from airborne LiDAR point clouds. *Remote Sensing*, 11:2373.

Lin, Y.-C. and Habib, A. (2021). Quality control and crop characterization framework for multi-temporal uav lidar data over mechanized agricultural fields. *Remote Sensing of Environment*, 256:112299.

Mughal, M. H., Khokhar, M. J., and Shahzad, M. (2021). Assisting uav localization via deep contextual image matching. *IEEE Journal of Selected Topics in Applied Earth Observations and Remote Sensing*, 14:2445–2457.

Segal, A., Haehnel, D., and Thrun, S. (2009). Generalized-icp. In *Robotics: science and systems*, volume 2, page 435.

Shabani, M., Gholami, A., and Davari, N. (2015). Asynchronous direct kalman filtering approach for underwater integrated navigation system. *Nonlinear Dynamics*, 80(1):71–85.

Souza Neto, P., Pereira, N. S., and Thé, G. A. P. (2018). Improved Cloud Partitioning Sampling for Iterative Closest Point: Qualitative and Quantitative Comparison Study. In *15th International Conference on Informatics in Control, Automation and Robotics*.

Vacca, G., Furfaro, G., and Dessi, A. (2018). The use of the uav images for the building 3d model generation. *The International Archives of the Photogrammetery, Remote Sensing and Spatial Information Sciences*, pages 217–223.

Wallace, L., Lucieer, A., Watson, C., and Turner, D. (2012). Development of a UAV-LiDAR system with application to forest inventory. *Remote Sensing*, 4(6):1519–1543.

Wang, J., Xu, L., Fan, Y., Liu, X., Tian, Z., Wang, X., and Cheng, Y. (2018). A method for compensating platform attitude fluctuation for helicopter-borne LiDAR: Performance and effectiveness. *Measurement*, 125:37–47.

Wang, J., Xu, L., Li, X., and Tian, X. (2011). Simulation on impact of random attitude measurement errors on point cloud and 3D image of ALS. In *2011 IEEE International Conference on Imaging Systems and Techniques*, pages 60–64.

Yang, J., Li, H., Campbell, D., and Jia, Y. (2016). Go-ICP: A Globally Optimal Solution to 3D ICP Point-Set Registration. *IEEE Transactions on Pattern Analysis and Machine Intelligence*.

Zhang, W., Yang, D., Li, Y., and Xu, W. (2020). Portable 3D laser scanner for volume measurement of coal pile. In *Communication, Signal Processing, and Systems. Lecture Notes in Electrical Engineering*, volume 517, pages 340–347.